Unveiling Two Electron-Transport Modes in Oxygen-Deficient TiO 2 Nanowires and Their Influence on Photoelectrochemical Operation

ARTICLE *in* JOURNAL OF PHYSICAL CHEMISTRY LETTERS · AUGUST 2014

Impact Factor: 7.46 · DOI: 10.1021/jz5014505

5 AUTHORS, INCLUDING:

Haining Chen
The Hong Kong University of Science and Tec…
42 PUBLICATIONS **503** CITATIONS
SEE PROFILE

Zhanhua Wei
The Hong Kong University of Science and Tec…
40 PUBLICATIONS **551** CITATIONS
SEE PROFILE

Keyou Yan
The Chinese University of Hong Kong
49 PUBLICATIONS **1,333** CITATIONS
SEE PROFILE

Shihe Yang
The Hong Kong University of Science and Tec…
378 PUBLICATIONS **11,011** CITATIONS
SEE PROFILE

THE JOURNAL OF PHYSICAL CHEMISTRY Letters

Letter

pubs.acs.org/JPCL

Unveiling Two Electron-Transport Modes in Oxygen-Deficient TiO_2 Nanowires and Their Influence on Photoelectrochemical Operation

Haining Chen, Zhanhua Wei, Keyou Yan, Yang Bai, and Shihe Yang*

Department of Chemistry, William Mong Institute of Nano Science and Technology, The Hong Kong University of Science and Technology, Clear Water Bay, Kowloon, Hong Kong

Supporting Information

ABSTRACT: Introducing oxygen vacancies (V_O) into TiO_2 materials is one of the most promising ways to significantly enhance light-harvesting and photocatalytic efficiencies of photoelectrochemical (PEC) cells for water splitting among others. However, the nature of electron transport in V_O-TiO_2 nanostructures is not well understood, especially in an operating device. In this work, we use the intensity-modulated photocurrent spectroscopy technique to study the electron-transport property of V_O-TiO_2 nanowires (NWs). It is found that the electron transport in pristine TiO_2 NWs displays a single trap-limited mode, whereas two electron-transport modes were detected in V_O-TiO_2 NWs, a trap-free transport mode at the core, and a trap-limited transport mode near the surface. The considerably higher diffusion coefficient (D_n) of the trap-free transport mode grants a more rapid electron flow in V_O-TiO_2 NWs than that in pristine TiO_2 NWs. This electron-transport feature is expected to be common in other oxygen-deficient metal oxides, lending a general strategy for promoting the PEC device performance.

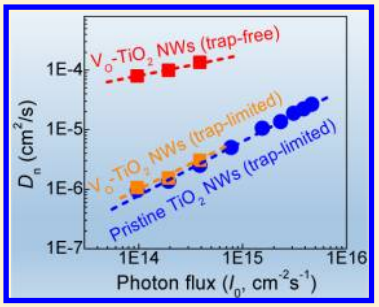

SECTION: Energy Conversion and Storage; Energy and Charge Transport

TiO_2 has been widely studied as an important photoelectrode material for photoelectrochemical (PEC) water splitting because of its high chemical stability, nontoxicity, and low cost.[1−20] However, the large band gap (3.0 eV for rutile) limits its light absorption within the ultraviolet light region, leading to the maximum theoretical conversion efficiency of only about 2.2%.[21,22] Besides, large electrical biases are usually needed to enable charge separation and to minimize electron−hole recombination in TiO_2.[17] As a result, the previously reported conversion efficiencies of TiO_2 photoelectrodes are still well below the theoretical expectation. To overcome these drawbacks, many efforts have been made to narrow the band gap and/or to minimize recombination losses.

Recently, introducing oxygen vacancies (V_O) into TiO_2 (through heat treatment in H_2 gas,[5,23] electrochemical reduction,[8,24] chemical reduction (e.g., $NaBH_4$[10] and $TiCl_3$[9]), melted aluminum reduction,[7,16] and flame reduction[9]) has been under intense investigation to improve the light-harvesting and photocatalytic properties. The energy level of V_O is located at 0.75 and 1.2 eV below the CB edge, which could enhance the visible light absorption.[22,23] In addition, it was proposed that the V_O act as electron donors to facilitate charge transport and separation, resulting in a significant improvement of incident photon-to-current conversion efficiency (IPCE) (near unity) in its characteristic absorption.[5,22] By combining the strategies of introducing V_O and doping (with N and S elements),[7,25] the PEC performance of TiO_2 could be further improved in the visible light region. Similar results have also been observed when V_O were introduced into other metal oxides (α-Fe_2O_3, WO_3, ZnO, and $BiVO_4$) to improve PEC performance.[9,26,27]

It has been suggested that the improvement in electron transport signals an important positive effect of V_O on the PEC performance of TiO_2 photoelectrodes. However, to our knowledge, little experimental data has been obtained in the PEC system to support this proposition. In this work, the electron-transport property of the oxygen-deficient TiO_2 materials (nanowires), V_O-TiO_2 NWs, was evaluated by using the intensity-modulated photocurrent spectroscopy (IMPS) technique in the PEC system. Interestingly, two distinct electron-transport modes were detected in the V_O-TiO_2 NWs, a trap-free mode at the core and a trap-limited mode near the surface, while only a trap-limited mode was observed for the pristine TiO_2 NWs. Moreover, the considerably larger diffusion coefficient (D_n) of the trap-free transport mode grants a more rapid electron transport in V_O-TiO_2 NWs than that in pristine TiO_2 NWs.

TiO_2 NWs with an average length of ∼2 μm were grown on FTO glass using a typical hydrothermal method,[4,28] as shown in Figure 1A. The diameter of the TiO_2 NWs ranges from 100 to 250 nm. An electrochemical reduction method was used to prepare V_O-TiO_2 NWs. Briefly, the pristine TiO_2 NWs were reduced in an aqueous solution of 1 M Na_2SO_4 at −1.8 V versus Ag/AgCl for 5−10 min.[8,24]

X-ray photoelectron spectroscopy (XPS) in Figure 1B shows the chemical composition and oxidation state of titanium in the pristine TiO_2 NWs and V_O-TiO_2 NWs. The high-resolution

Received: July 12, 2014
Accepted: August 5, 2014
Published: August 5, 2014

   dx.doi.org/10.1021/jz5014505 | J. Phys. Chem. Lett. 2014, 5, 2890−2896

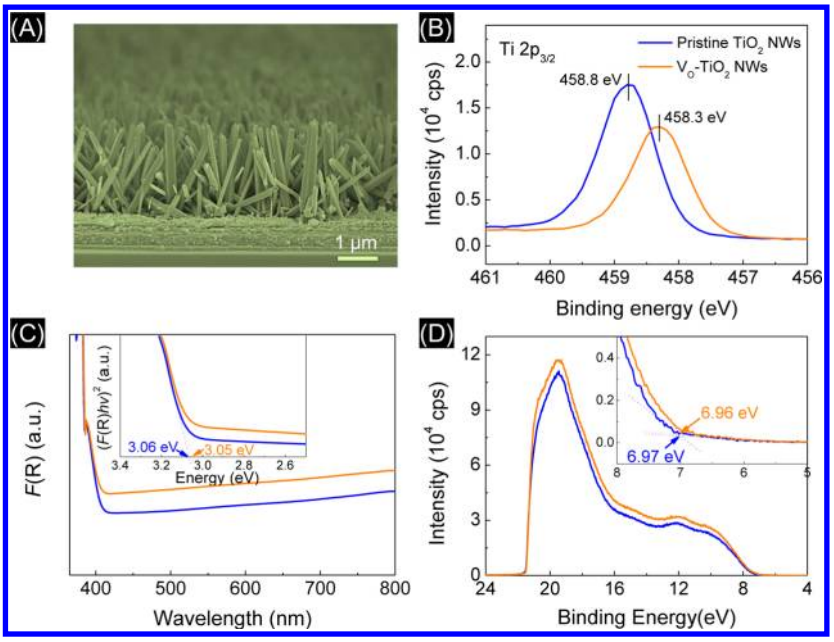

Figure 1. Characterizations of the pristine TiO_2 NWs and V_O-TiO_2 NWs. (A) A representative cross-sectional SEM image of pristine TiO_2 NWs. (B) XPS spectra of the Ti $2p_{3/2}$ core level. (C) Diffuse reflectance UV−vis absorption spectra. Inset are the plots of $(F(R)h\nu)^2 - h\nu$, from which E_g values of 3.06 and 3.05 eV are obtained for pristine TiO_2 NWs and V_O-TiO_2 NWs, respectively. (D) UPS spectra of pristine TiO_2 NWs and V_O-TiO_2 NWs, from which similar E_{VB} values of −6.97 and −6.96 eV are obtained.

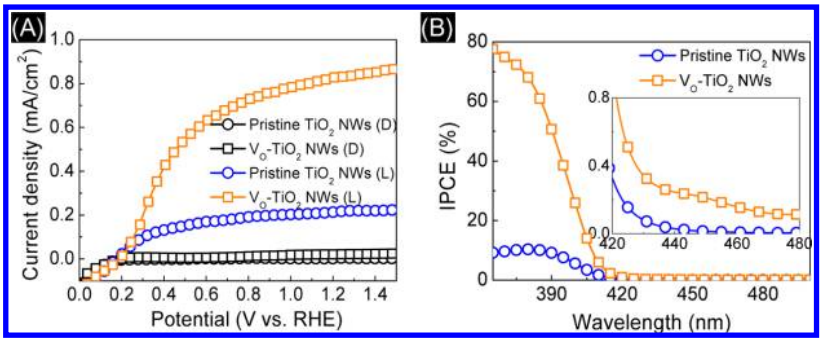

Figure 2. PEC performance of the pristine TiO_2 NWs and V_O-TiO_2 NWs in the aqueous solution of 1 M KOH: (A) $J-V$ curves under dark (D) and light illumination (L) (1 sun, 100 mW/cm^2) and (B) IPCE spectra. The inset shows the zoomed IPCE spectra in the wavelength region from 420 to 480 nm.

spectra of the Ti $2p_{3/2}$ core level from the pristine TiO_2 NWs and V_O-TiO_2 NWs are presented in Figure 1B. The pristine TiO_2 NWs sample shows the peak at 458.8 eV, while a red shift in binding energy to 458.3 eV is observed for V_O-TiO_2 NWs, indicating the different chemical environment for titanium cations. As reported in the literature,[10,29,30] this change was attributed to the presence of Ti^{3+} cations created by reduction processes, which leads to an increment in electron density and thus a weaker binding effect.[10,28,29]

Figure 1C shows the diffuse reflectance UV−vis absorption spectra of the pristine TiO_2 NWs and V_O-TiO_2 NWs. The absorption thresholds for the pristine TiO_2 NWs and V_O-TiO_2 NWs, corresponding to the electronic transition from the valence band (VB) to the conduction band (CB), are similar. The $(F(R)h\nu)^2 - h\nu$ plots in the inset of Figure 1C indicate that the band gap (E_g) values for pristine TiO_2 NWs and V_O-TiO_2 NWs are about 3.06 and 3.05 eV, respectively. Besides, V_O-TiO_2 NWs exhibit a remarkably enhanced absorption in the visible light region in comparison with pristine TiO_2 NWs, which can be attributed to the electronic transition from the VB to the V_O states (located at 0.75 and 1.2 eV below the CB edge) and/or from these states to the CB.[22,23] Ultraviolet photoelectron spectroscopy (UPS) results in Figure 1D indicate that the VB edge energies (E_{VB}) for the pristine TiO_2 NWs and V_O-TiO_2 NWs are also similar, namely, about −6.97 and −6.96 eV, respectively, with reference to the vacuum level. Therefore, electrochemical reduction processes hardly change the VB and CB edges, but the generated V_O states enhance the absorption in the visible light region.

In our electrochemical and PEC experiments, a standard three-electrode system was used with pristine TiO_2 NWs or V_O-TiO_2 NWs, Pt mesh, and a Ag/AgCl electrode as the working, counter, and reference electrodes, respectively. The electrolyte was an aqueous solution containing 1 M KOH. The potential was measured against a Ag/AgCl reference electrode and converted to a reversible hydrogen electrode (RHE) potential by using the Nernst equation[31]

$$E_{RHE} = E_{Ag/AgCl} + 0.059\,pH + 0.1976\,V \quad (1)$$

As shown in Figure 2A, obvious photocurrent is detected under light illumination for both photoelectrodes, and V_O-TiO_2 NWs presents significantly higher photocurrent density than

dx.doi.org/10.1021/jz5014505 | J. Phys. Chem. Lett. 2014, 5, 2890−2896

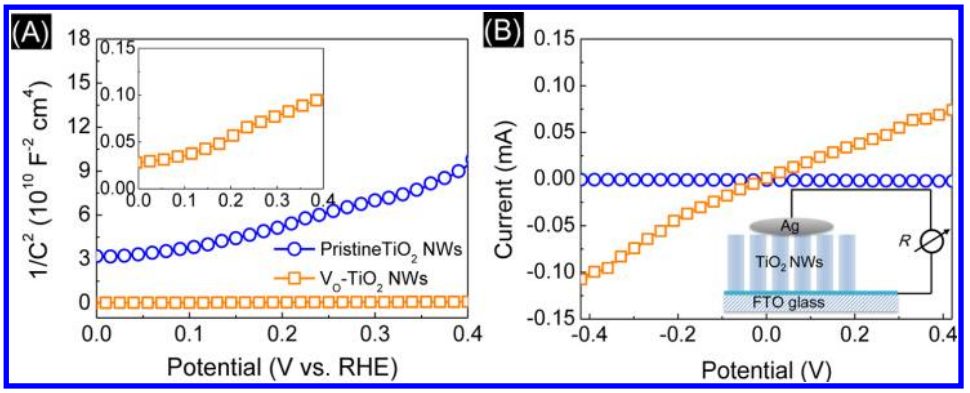

Figure 3. Electrical transport properties of the pristine TiO_2 NWs and V_O-TiO_2 NWs: (A) M−S plots obtained from the aqueous solution of 1 M KOH and (B) two-point current−potential (I−V) curves. The left inset zooms in on the M−S plot of the V_O-TiO_2 NWs, while the right inset schematizes the I−V measurement setup under dark conditions.

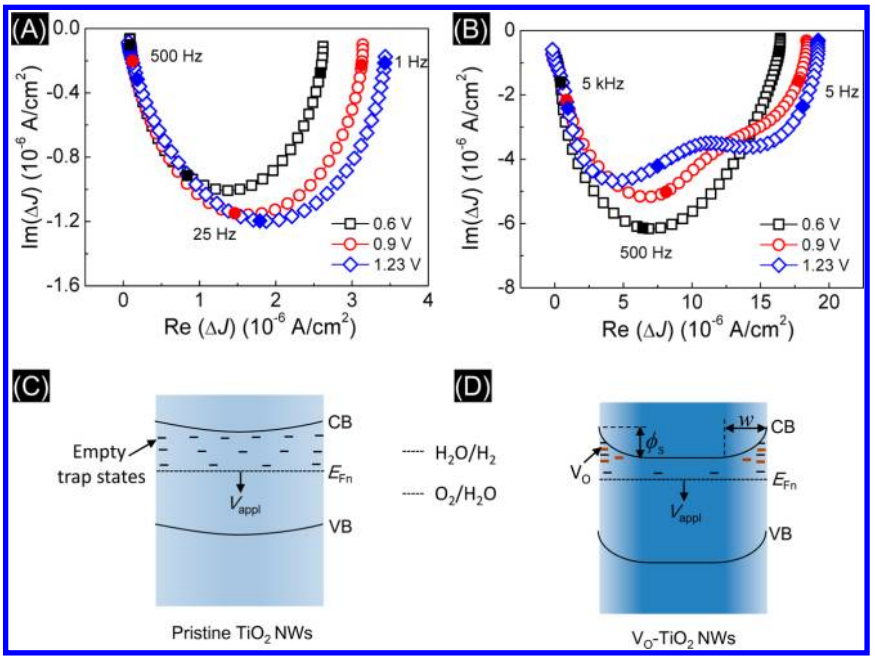

Figure 4. Electron-transport behaviors of pristine TiO_2 NWs and V_O-TiO_2 NWs in the PEC system used for the J−V curve measurement at different V_{appl}. IMPS complex plane plots of the (A) pristine TiO_2 NWs and (B) V_O-TiO_2 NWs at different V_{appl} versus RHE. Some specific frequencies are indicated by the filled symbols. Schematic energy diagrams and trap state distributions of (C) pristine TiO_2 NWs and (D) V_O-TiO_2 NWs.

pristine TiO_2 NWs. As expected, the maximum power conversion efficiency (PCE) achieved by V_O-TiO_2 NWs is only 0.11%, while it increases remarkably to 0.40% for V_O-TiO_2 NWs. This drastic improvement in PCE demonstrates that the electrochemical reduction is a promising method for preparing V_O-TiO_2 photoelectrodes for PEC, considering especially that it was conducted at room temperature and took only 10 min.

To find the origin of the PEC enhancement, IPCE was used to characterize the photoconversion efficiency at different wavelengths. IPCE is defined as[32]

$$\mathrm{IPCE} = \frac{(1240 \times I_{PH})}{(\lambda \times P_{light})} \quad (2)$$

where I_{PH} is the generated photocurrent density, λ the incident light wavelength, P_{light} the photon flux, and 1240 a unit correction factor. The IPCE spectra measured at 1.23 V versus RHE are presented in Figure 2B. Compared with the pristine TiO_2 NWs, the V_O-TiO_2 NWs exhibit a significantly enhanced photoactivity over the entire UV region, for example, the IPCE values at the wavelength below 390 nm are higher than 50%. The zoomed IPCE spectra from 420 to 480 nm in the inset of Figure 2B indicate that the photoactivity of the V_O-TiO_2 NWs in the visible light region is also improved, but the IPCE values are lower than 1%. Therefore, the enhanced photocurrent and PCE for the V_O-TiO_2 NWs prepared by electrochemical reduction are mainly attributed to the improved IPCE in the UV region, which is consistent with the results using materials prepared by other methods.[5,7−10,16,24] Together, the significantly enhanced PEC performance of the V_O-TiO_2 NWs should be mainly accounted for by the improved charge separation and electron transport.

To study the electron-transport properties, Mott−Schottky (M−S) plots and two-point conductivity were first measured. M−S plots in Figure 3A show positive slopes for both pristine TiO_2 NWs and V_O-TiO_2 NWs, indicating their n-type semiconductor behaviors, and V_O-TiO_2 NWs exhibits a much smaller slope than pristine TiO_2 NWs, implying a much higher free charge carrier density. Using the following equation[19]

dx.doi.org/10.1021/jz5014505 | J. Phys. Chem. Lett. 2014, 5, 2890−2896

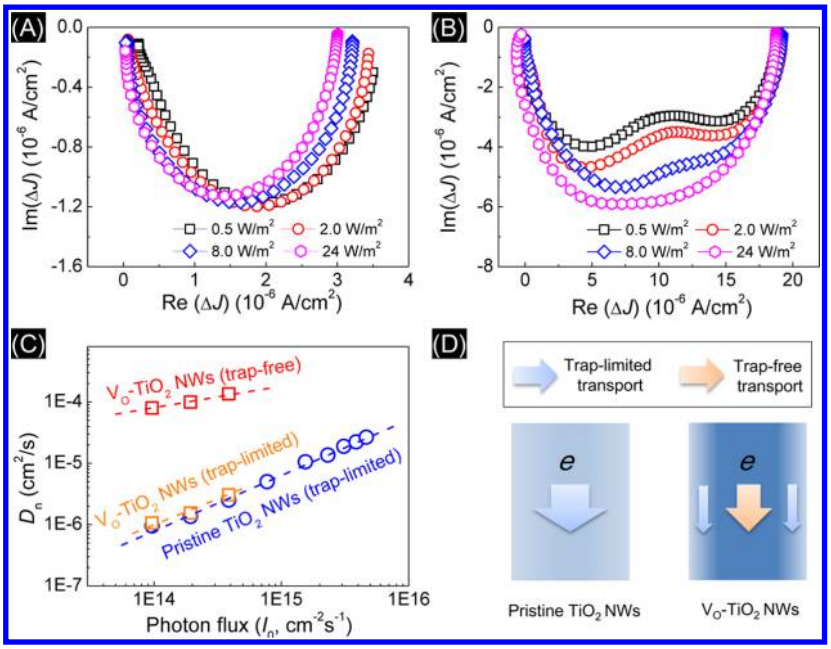

Figure 5. Electron-transport properties of the pristine TiO_2 NWs and V_O-TiO_2 NWs in the PEC system used for the $J-V$ curve measurement at different I_0. IMPS complex plane plots of (A) pristine TiO_2 NWs and (B) V_O-TiO_2 NWs at different I_0. (C) Extracted D_n from the IMPS complex plane plots. (D) Schematic of the possible electron-transport behaviors in pristine TiO_2 NWs and V_O-TiO_2 NWs; pristine TiO_2 NWs display a trap-limited electron-transport mode, while V_O-TiO_2 NWs exhibit two electron-transport modes (a trap-free mode at the core and a trap-limited mode near the surface).

$$N_c = \left(\frac{2}{e_0 \varepsilon \varepsilon_0}\right)\left[\frac{d(1/C^2)}{dV}\right]^{-1} \quad (3)$$

where e_0 is the electron charge, ε the dielectric constant of rutile TiO_2, ε_0 the permittivity of vacuum, N_c the carrier density, and V the applied potential. The N_c values for the pristine TiO_2 NWs and V_O-TiO_2 NWs are calculated to be about 4.56×10^{18} and 3.31×10^{20} cm^{-3}, respectively. A higher N_c of the latter indicates a larger upward shift of the Fermi level, resulting in a significant energy band bending at the surface of V_O-TiO_2 NWs,[22,33,34] which will facilitate charge separation at the TiO_2 NWs/electrolyte interface. In addition, the higher N_c in semiconductors also improves the charge conductivity, which has been widely suggested to enhance the PEC performance.[5,22]

Two-point current−potential ($I-V$) curves in Figure 3B were measured using the electrode configuration shown in the inset under dark conditions. It can be readily seen that the V_O-TiO_2 NWs present a considerably higher conductivity than the pristine TiO_2 NWs. Therefore, these results suggest that the electrochemical reduction greatly increases the N_c and hence considerably improves the overall electron-transport property.

To study the electron-transport properties of the V_O-TiO_2 NWs in the PEC system, the IMPS technique was applied. The IMPS complex plane plots for the pristine TiO_2 NWs and the V_O-TiO_2 NWs at different applied voltages (V_{appl}) are shown in Figure 4A and B, respectively, in which the photoelectrodes were illuminated with a blue-light-emitting diode (λ_{max} = 385 nm) at a light intensity of 2 W/m^2. As shown in Figure 4A, there is only one distinct flattened semicircle regardless of V_{appl} (from 0.6 to 1.23 V versus RHE) for the pristine TiO_2 NWs, suggesting only one obvious electron-transport mode. As V_{appl} increases, the frequency at the nadir of the semicircle (f_{min}) increases. The electron-transport time (t_d) can be calculated from the relation[35,36]

$$t_d = \frac{1}{2\pi f_{min}} \quad (4)$$

Therefore, the electron transport in the pristine TiO_2 NWs is accelerated as V_{appl} increases, in accord with the change of the photocurrent with V_{appl} on the $J-V$ curve (see Figure 2A).

For the V_O-TiO_2 NWs, however, the IMPS complex plane plot exhibits a single slightly deformed flattened semicircle at low V_{appl} (0.6 V versus RHE). Note that the f_{min} is about hundreds of Hz, much higher than those for the pristine TiO_2 NWs (tens of Hz) at different V_{appl}, indicating the much higher electron-transport rate in the V_O-TiO_2 NWs. As V_{appl} increases from 0.9 to 1.23 V, two flattened semicircles becomes more and more distinct at high and low frequencies, implying two significantly different electron-transport modes that are present in the V_O-TiO_2 NWs. In other words, a fraction of the electrons are collected with a smaller transport time constant, while the remaining electrons are collected with a larger time constant.

As is well-known, electrons diffusing in TiO_2 nanostructures could be multiply captured by trap states that usually distribute exponentially below the CB.[37−40] Such a trapping/detrapping process (multiple trapping model) is a dominant mechanism for electron transport in the TiO_2 nanostructures, and as proposed in the literature, two transport modes should be observed when the transport of a fraction of electrons is governed by trapping/detrapping events (trap-limited mode), whereas the transport of the remaining electrons is almost uninfluenced by the trapping/detrapping events (trap-free mode).[41−44]

To better understand the possible two electron-transport modes in the V_O-TiO_2 NWs, the energy band diagram and the trap state distribution of the pristine TiO_2 NWs and the V_O-TiO_2 NWs in the PEC system are schematically shown in Figure 4C and D, respectively. Due to the low electron density, the pristine TiO_2 NWs would be fully depleted (Figure 4C) in

dx.doi.org/10.1021/jz5014505 | J. Phys. Chem. Lett. 2014, 5, 2890−2896

a PEC cell,[22] leading to a similar distribution of empty trap states along the radial direction. As such, a large number of empty deep trap states will be generated because F_n is well below the CB, and electron transport in the entire TiO_2 NWs will be strongly governed by trapping/detrapping events according to the multiple trapping model.[37,38]

Regarding the V_O-TiO_2 NWs, however, the considerably higher N_c is reflected by the raised Fermi level toward the CB edge. In a PEC system, the V_O-TiO_2 NWs are expected to support a strong energy band bending (see Figure 4D).[22,33] As a result, the empty trap states at the core become close to the CB edge (shallow trap states), whereas more deep empty trap states are located near the surface.[42] We have implicitly assumed that the V_O states are mainly generated near the surface of the NWs, which is reasonable because the electrochemical treatment is in itself a surface process. Upon light illumination, the strong band bending enables efficient charge separation and will draw more photoelectrons toward the core to fill the shallow trap states.[22] As a consequence, there will be a higher density of free electrons at the core of the V_O-TiO_2 NWs, and thereby, the trapping/detrapping process will cease to dominate the electron transport at the core. Meanwhile, electron transport near the surface should still be governed by trapping/detrapping events due to the presence of deep trap state. Besides, the emptied shallow V_O states in high density near the NW surface may further accentuate the trapping/detrapping transport in the surface region.

As shown in Figure 4D, increasing V_{appl} will lower the F_n and increase the depth of the depletion zone (ϕ_s, aka, reduced potential) and thus draw more electrons toward the core and generate deeper empty trap states near the surface.[22] According to the following relation[45,46]

$$w = (2\phi_s)^{1/2} L_D \tag{5}$$

where w represents the width of the depletion zone and $L_D = (\varepsilon_0 \varepsilon k_B T/e^2 N_d)^{1/2}$ is the Debye length, w increases with ϕ_s, thinning down the unbending region at the core and thereby resulting in a higher electron density. Consequently, the trap-free transport mode down the core and the trap-limited transport mode near the surface will become more distinct with increasing V_{appl}, as is observed.

To gain a deeper insight into the electron-transport behaviors of pristine TiO_2 NWs and V_O-TiO_2 NWs in the PEC system, we recorded background illumination light density (I_0)-dependent IMPS complex plane plots at V_{appl} = 1.23 V, as shown in Figure 5A and B. Only a single flattened semicircle is observed in the IMPS complex plane plots for the pristine TiO_2 NWs, whereas the V_O-TiO_2 NWs show two flattened semicircles at low I_0, which are gradually merged into each other with increasing I_0.

The D_n for different transport modes were calculated by using the following relation[36,47]

$$D_n = \frac{L^2}{2.35 t_d} \tag{6}$$

where L is the film thickness and t_d is calculated according to eq 4 using the f_{min} of different characteristic flattened semicircles. Figure 5C shows the dependence of D_n on I_0 for the pristine TiO_2 NWs and the V_O-TiO_2 NWs in the double-logarithmic representation. In the multiple trapping model, D_n is expressed as[48]

$$D_n = \frac{D_0}{(1 + \partial n_L/\partial n_c)} \approx \left(\frac{N_c^{\alpha}}{\alpha N_L}\right) n_c^{1-\alpha} D_0 \tag{7}$$

where D_0 is the diffusion coefficient in the trap-free system, n_c is the density of CB electrons, n_L is the density of localized electrons in traps, N_c is the effective density of CB states, N_L is the density of trap states, and $\alpha = T/T_0$ ($0 < \alpha < 1$; T_0 is the tailing parameter of exponential distribution). According to eq 7, $D_n \propto I_0^{1-\alpha}$ assuming that $n_c \propto I_0$. The fitting of the data in Figure 5C reveals a strong dependence of D_n on I_0 ($D_n \propto I_0^{0.86}$) for pristine TiO_2 NWs, which indeed implies a typical trap-limited electron-transport mode.[37,47]

For the V_O-TiO_2 NWs, the D_n determined from the low-frequency flattened semicircles also exhibits a strong dependence on I_0 ($D_n \propto I_0^{0.60}$), confirming the trap-limited transport nature near the NW surface. On the other hand, the D_n determined from the high-frequency flattened semicircles of the V_O-TiO_2 NWs is about 2 orders of magnitude higher than those determined for the low-frequency flattened semicircles. Those D_n values present a much weaker dependence on I_0 ($D_n \propto I_0^{0.38}$), which is typical of the trap-free transport mode, because trap states at the core are significantly occupied.[42,44,49] The weak dependence of D_n on I_0 is very beneficial for low light intensity operation, which is confirmed by the higher photocurrent density ratios of V_O-TiO_2 NWs to pristine TiO_2 NWs at lower light intensities (see Figure S5, Supporting Information). The strong and weak dependences of D_n on I_0 for the trap-limited mode and the trap-free mode, respectively, lead to the gradual overlay of their corresponding flattened semicircles as I_0 increases (Figure 5B) as the trap states are gradually filled out. Thus, by varying the electrochemical reduction duration, the D_n for the trap-limited mode and trap-free mode could be effectively controlled (Figure S6, Supporting Information).

On the basis of the analysis above, possible different electron-transport behaviors in the pristine TiO_2 NWs and the V_O-TiO_2 NWs can be proposed in Figure 5D. Namely, the pristine TiO_2 NWs display a single trap-limited mode, whereas the V_O-TiO_2 NWs could exhibit two distinct electron-transport modes, a trap-free transport at the core and a trap-limited transport near the surface. These two transport modes tend to overlay with each other as V_{appl} decreases or I_0 increases. As one would expect, the considerably larger D_n of the trap-free transport mode grants a more rapid electron transport in the V_O-TiO_2 NWs than that in the pristine TiO_2 NWs.

In summary, we have investigated the electron-transport property of the V_O-TiO_2 NWs by the IMPS technique using the pristine TiO_2 NWs as a reference for comparison in the PEC system. A single trap-limited electron-transport mode was observed in TiO_2 NWs, while two electron-transport modes were detected in V_O-TiO_2 NWs, a trap-free mode at the core and a trap-limited mode near the surface. These two modes could be distinguished at high V_{appl} and low illumination light intensity but tended to overlay with each other at low V_{appl} or high illumination light intensity. Due to considerably larger D_n for the trap-free transport mode, electron transport in V_O-TiO_2 NWs was found to be more rapid than that in TiO_2 NWs. It is expected that this electron-transport model in TiO_2 nanowires should also be applicable to other oxygen-deficient metal oxides, such as α-Fe_2O_3, WO_3, ZnO, and $BiVO_4$.

dx.doi.org/10.1021/jz5014505 | J. Phys. Chem. Lett. 2014, 5, 2890−2896

■ ASSOCIATED CONTENT

Supporting Information

Experimental details and Figures S1−S6, including details of the growth of TiO_2 NWs, preparation of V_O-TiO_2 NWs, characterizations, photoelectrochemical testing, XRD patterns, O1s core-level XPS spectra, t_d, the photocurrent density, and electron transport properties for TiO_2 NWs and V_O-TiO_2 NWs as well as the relationship between the power conversion efficiency and applied potential. This material is available free of charge via the Internet at http://pubs.acs.org.

■ AUTHOR INFORMATION

Corresponding Author

*E-mail: chsyang@ust.hk.

Notes

The authors declare no competing financial interest.

■ ACKNOWLEDGMENTS

This work was supported by the HK-RGC General Research Funds (GRF No. HKUST 606511 and 605710).

■ REFERENCES

(1) Fujishima, A. Electrochemical Photolysis of Water at a Semiconductor Electrode. *Nature* **1972**, *238*, 37−38.

(2) Feng, X.; Zhu, K.; Frank, A. J.; Grimes, C. A.; Mallouk, T. E. Rapid Charge Transport in Dye-Sensitized Solar Cells Made from Vertically Aligned Single-Crystal Rutile TiO_2 Nanowires. *Angew. Chem., Int. Ed.* **2012**, *51*, 2727−2730.

(3) Wolcott, A.; Smith, W. A.; Kuykendall, T. R.; Zhao, Y.; Zhang, J. Z. Photoelectrochemical Water Splitting Using Dense and Aligned TiO_2 Nanorod Arrays. *Small* **2009**, *5*, 104−111.

(4) Cho, I. S.; Chen, Z.; Forman, A. J.; Kim, D. R.; Rao, P. M.; Jaramillo, T. F.; Zheng, X. Branched TiO_2 Nanorods for Photoelectrochemical Hydrogen Production. *Nano Lett.* **2011**, *11*, 4978−4984.

(5) Wang, G.; Wang, H.; Ling, Y.; Tang, Y.; Yang, X.; Fitzmorris, R. C.; Wang, C.; Zhang, J. Z.; Li, Y. Hydrogen-Treated TiO_2 Nanowire Arrays for Photoelectrochemical Water Splitting. *Nano Lett.* **2011**, *11*, 3026−3033.

(6) Pu, Y. C.; Wang, G.; Chang, K. D.; Ling, Y.; Lin, Y. K.; Fitzmorris, B. C.; Liu, C. M.; Lu, X.; Tong, Y.; Zhang, J. Z.; et al. Au Nanostructure-Decorated TiO_2 Nanowires Exhibiting Photoactivity across Entire UV−Visible Region for Photoelectrochemical Water Splitting. *Nano Lett.* **2013**, *13*, 3817−3823.

(7) Yang, C.; Wang, Z.; Lin, T.; Yin, H.; Lu, X.; Wan, D.; Xu, T.; Zheng, C.; Lin, J.; Huang, F.; et al. Core−Shell Nanostructured "Black" Rutile Titania as Excellent Catalyst for Hydrogen Production Enhanced by Sulfur Doping. *J. Am. Chem. Soc.* **2013**, *135*, 17831−17838.

(8) Zhang, Z.; Hedhili, M. N.; Zhu, H.; Wang, P. Electrochemical Reduction Induced Self-Doping of Ti^{3+} for Efficient Water Splitting Performance on TiO_2 Based Photoelectrodes. *Phys. Chem. Chem. Phys.* **2013**, *15*, 15637−15644.

(9) Cho, I. S.; Logar, M.; Lee, C. H.; Cai, L.; Prinz, F. B.; Zheng, X. Rapid and Controllable Flame Reduction of TiO_2 Nanowires for Enhanced Solar Water-Splitting. *Nano Lett.* **2014**, *14*, 24−31.

(10) Kang, Q.; Cao, J.; Zhang, Y.; Liu, L.; Xu, H.; Ye, J. Reduced TiO_2 Nanotube Arrays for Photoelectrochemical Water Splitting. *J. Mater. Chem. A* **2013**, *1*, 5766−5774.

(11) Wang, Y.; Zhang, Y. Y.; Tang, J.; Wu, H.; Xu, M.; Peng, Z.; Gong, X. G.; Zheng, G. Simultaneous Etching and Doping of TiO_2 Nanowire Arrays for Enhanced Photoelectrochemical Performance. *ACS Nano* **2013**, *7*, 9375−9383.

(12) Feng, X.; Shankar, K.; Varghese, O. K.; Paulose, M.; Latempa, T. J.; Grimes, C. A. Vertically Aligned Single Crystal TiO_2 Nanowire Arrays Grown Directly on Transparent Conducting Oxide Coated Glass: Synthesis Details and Applications. *Nano Lett.* **2008**, *8*, 3781−3786.

(13) Park, J. H.; Kim, S.; Bard, A. J. Novel Carbon-Doped TiO_2 Nanotube Arrays with High Aspect Ratios for Efficient Solar Water Splitting. *Nano Lett.* **2006**, *6*, 24−28.

(14) Hwang, Y. J.; Hahn, C.; Liu, B.; Yang, P. Photoelectrochemical Properties of TiO_2 Nanowire Arrays: A Study of the Dependence on Length and Atomic Layer Deposition Coating. *ACS Nano* **2012**, *6*, 5060−5069.

(15) Liu, N.; Schneider, C.; Freitag, D.; Hartmann, M.; Venkatesan, U.; Müller, J.; Spiecker, E.; Schmuki, P. Black TiO_2 Nanotubes: Co-Catalyst Free Open-Circuit Hydrogen Generation. *Nano Lett.* **2014**, *14*, 3309−3313.

(16) Cui, H.; Zhao, W.; Yang, C.; Yin, H.; Lin, T.; Shan, Y.; Xie, Y.; Gu, H.; Huang, F. Black TiO_2 Nanotube Arrays for High-Efficiency Photoelectrochemical Water-Splitting. *J. Mater. Chem. A* **2014**, *2*, 8612−8616.

(17) Cowan, A. J.; Tang, J. W.; Leng, W. H.; Durrant, J. R.; Klug, D. R. Water Splitting by Nanocrystalline TiO_2 in a Complete Photoelectrochemical Cell Exhibits Efficiencies Limited by Charge Recombination. *J. Phys. Chem. C* **2010**, *114*, 4208−4214.

(18) Khan, S. U.; Al-Shahry, M.; Ingler, W. B. Efficient Photochemical Water Splitting by a Chemically Modified N-TiO_2. *Science* **2002**, *297*, 2243−2245.

(19) Walter, M. G.; Warren, E. L.; McKone, J. R.; Boettcher, S. W.; Mi, Q. X.; Santori, E. A.; Lewis, N. S. Solar Water Splitting Cells. *Chem. Rev.* **2010**, *110*, 6446−6473.

(20) Watanabe, A.; Kotake, Y.; Kamata, Y.; Chikamatsu, A.; Ueno, K.; Misawa, H.; Hasegawa, T. Photoelectrochemical Behavior of Self-Assembled Ag/Co Plasmonic Nanostructures Capped with TiO_2. *J. Phys. Chem. Lett.* **2013**, *5*, 25−29.

(21) Murphy, A. B.; Barnes, P. R. F.; Randeniya, L. K.; Plumb, I. C.; Grey, I. E.; Horne, M. D.; Glasscock, J. A. Efficiency of Solar Water Splitting Using Semiconductor Electrodes. *Int. J. Hydrogen Energy* **2006**, *31*, 1999−2017.

(22) Pesci, F. M.; Wang, G.; Klug, D. R.; Li, Y.; Cowan, A. J. Efficient Suppression of Electron−Hole Recombination in Oxygen-Deficient Hydrogen-Treated TiO_2 Nanowires for Photoelectrochemical Water Splitting. *J. Phys. Chem. C* **2013**, *117*, 25837−25844.

(23) Wheeler, D. A.; Ling, Y. C.; Dillon, R. J.; Fitzmorris, R. C.; Dudzik, C. G.; ZaV_Odivker, L.; Rajh, T.; Dimitrijevic, N. M.; Millhauser, G.; Bardeen, C.; et al. Probing the Nature of Bandgap States in Hydrogen-Treated TiO_2 Nanowires. *J. Phys. Chem. C* **2013**, *117*, 26821−26830.

(24) Lindquist, S.-E.; Lindgren, A.; Leygraf, C. Effects of Electrochemical Reduction of Polycrystalline TiO_2 Photoelectrodes in Acidic Solutions. *Sol. Energy Mater.* **1987**, *15*, 367−382.

(25) Hoang, S.; Berglund, S. P.; Hahn, N. T.; Bard, A. J.; Mullins, C. B. Enhancing Visible Light Photo-Oxidation of Water with TiO_2 Nanowire Arrays Via Cotreatment with H_2 and NH_3: Synergistic Effects between Ti^{3+} and N. *J. Am. Chem. Soc.* **2012**, *134*, 3659−3662.

(26) Wang, G. M.; Ling, Y. C.; Wang, H. Y.; Yang, X. Y.; Wang, C. C.; Zhang, J. Z.; Li, Y. Hydrogen-Treated WO_3 Nanoflakes Show Enhanced Photostability. *Energy Environ. Sci.* **2012**, *5*, 6180−6187.

(27) Wang, G. M.; Ling, Y. C.; Li, Y. Oxygen-Deficient Metal Oxide Nanostructures for Photoelectrochemical Water Oxidation and Other Applications. *Nanoscale* **2012**, *4*, 6682−6691.

(28) Liu, B.; Aydil, E. S. Growth of Oriented Single-Crystalline Rutile TiO_2 Nanorods on Transparent Conducting Substrates for Dye-Sensitized Solar Cells. *J. Am. Chem. Soc.* **2009**, *131*, 3985−3990.

(29) Lu, X. H.; Wang, G. M.; Zhai, T.; Yu, M. H.; Gan, J. Y.; Tong, Y. X.; Li, Y. Hydrogenated TiO_2 Nanotube Arrays for Supercapacitors. *Nano Lett.* **2012**, *12*, 1690−1696.

(30) Liang, Z.; Zheng, G.; Li, W.; Seh, Z. W.; Yao, H.; Yan, K.; Kong, D.; Cui, Y. Sulfur Cathodes with Hydrogen Reduced Titanium Dioxide Inverse Opal Structure. *ACS Nano* **2014**, *8*, 5249−5256.

(31) Qiu, Y.; Yan, K.; Deng, H.; Yang, S. Secondary Branching and Nitrogen Doping of ZnO Nanotetrapods: Building a Highly Active

Network for Photoelectrochemical Water Splitting. *Nano Lett.* **2012**, *12*, 407−413.
(32) Li, Y.; Zhang, J. Z. Hydrogen Generation from Photoelectrochemical Water Splitting Based on Nanomaterials. *Laser Photonics Rev.* **2009**, *4*, 517−528.
(33) Mora-Seró, I. n.; Fabregat-Santiago, F.; Denier, B.; Bisquert, J.; Tena-Zaera, R. n.; Elias, J.; Lévy-Clément, C. Determination of Carrier Density of ZnO Nanowires by Electrochemical Techniques. *Appl. Phys. Lett.* **2006**, *89*, 203117.
(34) Tornow, J.; Schwarzburg, K. Transient Electrical Response of Dye-Sensitized ZnO Nanorod Solar Cells. *J. Phys. Chem. C* **2007**, *111*, 8692−8698.
(35) van de Lagemaat, J.; Frank, A. J. Nonthermalized Electron Transport in Dye-Sensitized Nanocrystalline TiO_2 Films: Transient Photocurrent and Random-Walk Modeling Studies. *J. Phys. Chem. B* **2001**, *105*, 11194−11205.
(36) Peter, L.; Wijayantha, K. Electron Transport and Back Reaction in Dye Sensitised Nanocrystalline PhotoV$_O$ltaic Cells. *Electrochim. Acta* **2000**, *45*, 4543−4551.
(37) Van de Lagemaat, J.; Frank, A. Effect of the Surface-State Distribution on Electron Transport in Dye-Sensitized TiO_2 Solar Cells: Nonlinear Electron-Transport Kinetics. *J. Phys. Chem. B* **2000**, *104*, 4292−4294.
(38) Bisquert, J. Physical Electrochemistry of Nanostructured Devices. *Phys. Chem. Chem. Phys.* **2008**, *10*, 49−72.
(39) Leng, W. H.; Barnes, P. R. F.; Juozapavicius, M.; O'Regan, B. C.; Durrant, J. R. Electron Diffusion Length in Mesoporous Nanocrystalline TiO_2 Photoelectrodes During Water Oxidation. *J. Phys. Chem. Lett.* **2010**, *1*, 967−972.
(40) Bertoluzzi, L.; Herraiz-Cardona, I.; Gottesman, R.; Zaban, A.; Bisquert, J. Relaxation of Electron Carriers in the Density of States of Nanocrystalline TiO_2. *J. Phys. Chem. Lett.* **2014**, *5*, 689−694.
(41) Vanmaekelbergh, D.; de Jongh, P. E. Electron Transport in Disordered Semiconductors Studied by a Small Harmonic Modulation of the Steady State. *Phys. Rev. B* **2000**, *61*, 4699−4704.
(42) Wang, K. P.; Teng, H. Zinc-Doping in TiO_2 Films to Enhance Electron Transport in Dye-Sensitized Solar Cells under Low-Intensity Illumination. *Phys. Chem. Chem. Phys.* **2009**, *11*, 9489−96.
(43) Cao, F.; Oskam, G.; Meyer, G. J.; Searson, P. C. Electron Transport in Porous Nanocrystalline TiO_2 Photoelectrochemical Cells. *J. Phys. Chem.* **1996**, *100*, 17021−17027.
(44) Hsiao, P.-T.; Teng, H. Coordination of Ti^{4+} Sites in Nanocrystalline TiO_2 Films Used for Photoinduced Electron Conduction: Influence of Nanoparticle Synthesis and Thermal Necking. *J. Am. Ceram. Soc.* **2009**, *92*, 888−893.
(45) Schottky, W. Vereinfachte Und Erweiterte Theorie Der Randschicht-Gleichrichter. *Z. Phys. A: Hadrons Nucl.* **1942**, *118*, 539−592.
(46) Bisquert, J.; Garcia-Belmonte, G.; Fabregat-Santiago, F. Modelling the Electric Potential Distribution in the Dark in Nanoporous Semiconductor Electrodes. *J. Solid State Electrochem.* **1999**, *3*, 337−347.
(47) Kopidakis, N.; Benkstein, K. D.; van de Lagemaat, J.; Frank, A. J. Transport-Limited Recombination of Photocarriers in Dye-Sensitized Nanocrystalline TiO_2 Solar Cells. *J. Phys. Chem. B* **2003**, *107*, 11307−11315.
(48) Bisquert, J.; Vikhrenko, V. S. Interpretation of the Time Constants Measured by Kinetic Techniques in Nanostructured Semiconductor Electrodes and Dye-Sensitized Solar Cells. *J. Phys. Chem. B* **2004**, *108*, 2313−2322.
(49) Hsiao, P.-T.; Tung, Y.-L.; Teng, H. Electron Transport Patterns in TiO_2 Nanocrystalline Films of Dye-Sensitized Solar Cells. *J. Phys. Chem. C* **2010**, *114*, 6762−6769.